Organic Electronics 13 (2012) 1565–1568

Contents lists available at SciVerse ScienceDirect

Organic Electronics

journal homepage: www.elsevier.com/locate/orgel

Letter

Thermal properties of organic light-emitting diodes

Kevin J. Bergemann [a], Robert Krasny [b], Stephen R. Forrest [a,c,d,*]

[a] Department of Physics, University of Michigan, Ann Arbor, MI 48109, USA
[b] Department of Mathematics, University of Michigan, Ann Arbor, MI 48109, USA
[c] Department of Electrical Engineering and Computer Science, University of Michigan, Ann Arbor, MI 48109, USA
[d] Department of Materials Science and Engineering, University of Michigan, Ann Arbor, MI 48109, USA

ARTICLE INFO

Article history:
Received 10 February 2012
Received in revised form 28 April 2012
Accepted 3 May 2012
Available online 18 May 2012

Keywords:
Lighting
Convection
Conduction
Radiation

ABSTRACT

Thermal management is important for the efficient operation of organic light-emitting diodes (OLED, or PHOLED) at high brightness, with the device operating temperature influencing both lifetime and performance. We apply a transmission-matrix approach to analytically model the effects of thermal conduction, convection and radiation on OLED temperature. The model predictions match experiment without requiring the use of fitting parameters. This allows for the simulation of the thermal response of various device architectures, materials combinations and environmental factors under a variety of operating conditions. Using these simulations, we find that 87% of the heat is dissipated through the air space adjacent to the glass package cap. Furthermore, an air gap between the device cathode and cap provides a significant thermal impedance. Minimizing the thickness of the internal air gap can lead to nearly room temperature operation, even at very high brightness.

The high efficiency, large color gamut, and ease of manufacture of organic light-emitting diodes (OLEDs) have led to their practical application in flat panel displays [1]. More recently, large-area white OLEDs have also been found suitable for lighting applications, with devices already exceeding the efficiency of fluorescent panels [2,3]. However, the lifetime of OLEDs operated at the surface luminance required for lighting (3000 cd/m^2 or higher) is sensitive to temperature, with 1.65× longer lifetime for a decrease of 10 K [4]. Accurate methods for modeling and designing temperature-tolerant device structures and luminaries, therefore, are needed.

Here, we apply a recently introduced matrix method to quantify one-dimensional heat-transfer from the active region of a multi-layer, packaged OLED by fully describing the effects of conduction, convection and radiation. In an extension of previous work [5], we employ an analytical treatment for the effects of convection, allowing for an accurate determination of the packaged device thermal properties using no undetermined, free parameters. With this method, we describe approaches to minimizing the temperature increase in high-brightness OLEDs that are of particular interest in solid-state lighting applications.

As described previously [5,6], the transmission matrix approach employs Laplace transforms of the heat transfer equations. The solution to these equations through a single layer is represented using:

$$\begin{bmatrix} \widehat{T}_{i+1} \\ \widehat{Q}_{i+1} \end{bmatrix} = \begin{bmatrix} \cosh(\theta_i) & Z_i \sinh(\theta_i) \\ \frac{\sinh(\theta_i)}{Z_i} & \cosh(\theta_i) \end{bmatrix} \begin{bmatrix} \widehat{T}_i \\ \widehat{Q}_i \end{bmatrix} = \begin{bmatrix} A_i & B_i \\ C_i & D_i \end{bmatrix} \begin{bmatrix} \widehat{T}_i \\ \widehat{Q}_i \end{bmatrix} = [T(\theta_i)] \begin{bmatrix} \widehat{T}_i \\ \widehat{Q}_i \end{bmatrix}, \quad (1)$$

where $\widehat{T}_i(s)$ and $\widehat{Q}_i(s)$ are the Laplace transforms of the temperature and heat flux across the ith layer; $\theta_i = L_i\sqrt{C_i s/K_i}$ is the operational propagation constant, K_i is the thermal conductivity of the film, C_i is its volumetric heat capacity, L_i is the layer thickness, $Z_i = \sqrt{1/(K_i C_i s)}$ is the characteristic impedance, and A_i, B_i, C_i, and D_i are matrix elements that can be approximated by polynomial

* Corresponding author at: Department of Electrical Engineering and Computer Science, University of Michigan, Ann Arbor, MI 48109, USA.
E-mail address: stevefor@umich.edu (S.R. Forrest).

1566-1199/$ - see front matter © 2012 Elsevier B.V. All rights reserved.
http://dx.doi.org/10.1016/j.orgel.2012.05.004

expansions in the Laplace variable, s. Multiple layers are handled in one of two ways: a series of layers are treated as the product of the transmission matrices for the several films, while layers placed in parallel, or parallel heat channels such as conduction and thermal radiation, are treated by assuming that the incident heat flux splits between the two independent channels with no flow between them. This gives the final matrix as the sum of the channels:

$$\begin{bmatrix} \hat{Q}_1 \\ \hat{Q}_2 \end{bmatrix} = \sum_i \begin{bmatrix} \hat{Q}_{1i} \\ \hat{Q}_{2i} \end{bmatrix} = \sum_i \begin{bmatrix} A_i/B_i & -1/B_i \\ 1/B_i & -A_i/B_i \end{bmatrix} \begin{bmatrix} \hat{T}_1 \\ \hat{T}_2 \end{bmatrix} \tag{2}$$

The parallel and series channels are then combined to model heat transfer through arbitrary, multilayer, one-dimensional systems. Full OLED modeling also requires the inclusion of interface resistance [7] and the treatment of radiation and conduction as parallel heat transfer paths.

Previous work treated convective transfer from the device surface as an additional conductive layer whose thickness was used as a free parameter to match the model predictions to the measured data, thereby limiting its predictive capabilities. Here, we model convection using Newton's Law of Cooling [8,9], $Q_{\text{conv}} = h\Delta T$, where h is the convective heat transfer coefficient of the ambient, and ΔT is the temperature difference between the surface and ambient. For forced convection, h is a constant, while it is temperature-dependent for natural convection [9]. Now, Q_{conv} is derived from the Nusselt number, Nu whose form depends on the thermal environment and experimental geometry. For our analysis, we consider only the case of convection in the laminar flow regime from the upper surface of a heated, horizontally positioned packaged OLED. In this case [8], $Nu = hL/K_{\text{amb}} = 0.54Ra^{1/4}$, where L is the characteristic length of the system, K_{amb} is the thermal conductivity of the convective medium, and Ra is the Rayleigh number. Other orientations and geometries may be considered by inserting the appropriate expression for Nu. The Rayleigh number is then defined for a given convective medium, in our case air, as:

$$Ra = \frac{C_P \rho^2 g \beta (\Delta T) L^3}{\mu K_{amb}} \tag{3}$$

where C_P is the heat capacity at constant pressure of the convective medium, ρ is its density, μ the viscosity, g is the acceleration due to gravity, and β is the gas volume expansion coefficient. From the foregoing, we find that $Q \sim \Delta T^{5/4}$, which renders the Laplace transform of this equation mathematically intractable. However, the temperature rise for the devices studied is only 5–10 K even under the highest intensity operating conditions [4,5]. This small temperature change allows us to set the Rayleigh number to a constant, thereby linearizing Newton's Law of Cooling and greatly simplifying the analysis. The parameters used to calculate this term and the values of Ra and Nu are provided in Table 1. Applying this assumption for a simulated input power of 1 kW/m^2, we find that the device reaches a steady-state temperature of approximately 85 °C. If we then change the Rayleigh number by two orders of magnitude in the model, the steady-state temperature changes by only 2%, indicating that the model is largely insensitive to these changes.

Table 1
Rayleigh and Nusselt numbers at 25.5 °C.

Material	Density (kg/m^3)	Volume expansion (1/K)	Viscosity (kg/ms)	ΔT (K)
Air	1.18	3.35×10^{-3}	1.85×10^{-5}	6
Rayleigh number	9.0×10^3			
Nusselt number (horizontal plate)	5.3			

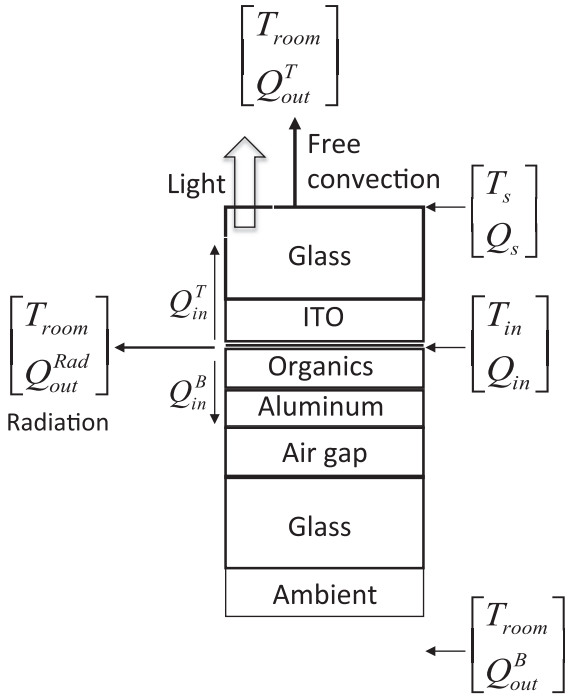

Fig. 1. Device structure of an OLED. Heat, Q_{in}, is input in the organic emission layer and then splits to flow toward the top, Q^T_{in}, and bottom, Q^B_{in}, device surfaces. T_{in} is then the temperature of the active layer, T_S and Q_S are the temperature and heat flow through the top device surface, T_{room} is the ambient temperature, and Q^T_{out}, Q^B_{out}, and $Q^{\text{Rad}}_{\text{out}}$ are the heat fluxes due to convection at the top surface, conduction at the bottom surface, and radiation, respectively.

Combining the analytical treatment of convection with the matrix method allows us to derive an expression for the device operating temperature, T_{in}, in terms of the input heat flux, Q_{in}, the heat transfer coefficient h, and the transmission matrix elements to yield:

$$T_{in} = -\frac{B_T^2\left(h + \frac{A_T}{B_T}\right)Q_{in}}{1 - B_T^2\left(h + \frac{A_T}{B_T}\right)\left(\frac{A_B}{B_B} + \frac{A_T}{B_T}\right)} \tag{4}$$

where $A_{\text{T,B}}$ and $B_{\text{T,B}}$ denote matrix elements corresponding to heat transfer through the top (T) and bottom (B) device surfaces (see Fig. 1).

We tested the model using a 25 cm^2, glass-encapsulated, green phosphorescent OLED (Universal Display Corp., Ewing, NJ) whose structure is shown schematically in Fig. 1. Its layer thicknesses and material thermal

Table 2
Thermal constants and layer thicknesses used in model.

Layer	Thickness (mm)	Heat capacity at constant pressure (10^2 J/kg K)	Thermal conductivity (W/K m)	References
Glass	0.7	8.2	1.3	[10,11]
ITO	1×10^{-3}	3.4	5.0	[5]
Organic active region	1×10^{-4}	17	0.2	[5]
Aluminum	1×10^{-4}	9.0	250	[10]
Air (internal gap)	1.9	10	0.026	[10]

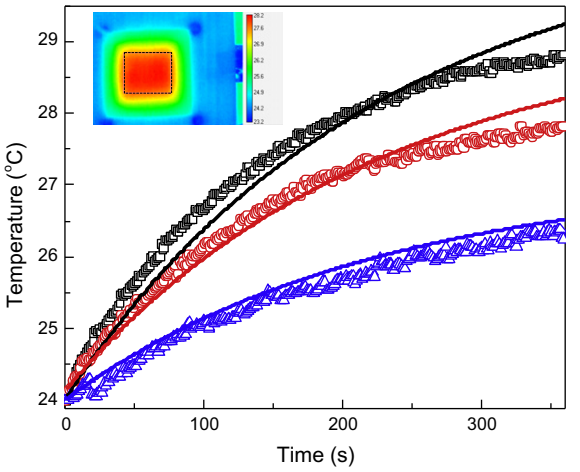

Fig. 2. Measured temperature of a 25 cm^2 green phosphorescent OLED at several different input current densities (points), compared to model predictions (lines). Data are taken at current densities of 2 mA/cm^2 (triangles), 3 mA/cm^2 (circles), and 4 mA/cm^2 (squares), with the current turned on at time $t = 0$. Inset: thermal image of an OLED after 6 min following the onset of a 3 mA/cm^2 current step. Current was injected around the device perimeter, which minimizes contact heating while resulting in a uniform thermal profile. The box in the figure shows the area which was averaged to obtain the device temperature. (For interpretation of the references to colour in this figure legend, the reader is referred to the web version of this article.)

constants are given in Table 2. Current density-vs.-voltage (J–V) characteristics were obtained using a Keithley 2400 source meter, while optical characteristics were measured using a calibrated reference detector. Thermal surface image measurements (Fig. 2, inset) were taken with a non-contact infrared camera (FLIR A325) inside a box with a black interior to eliminate stray reflections and to provide a stable thermal environment. Previous work has shown that the temperature difference between the upper surface and the organic light emitting layer (EML) is negligible [5]. Hence, we can assume that the thermal image temperature is the same as that of the EML. The input thermal power was calculated from the total input electrical power and the measured output optical power [5], Q_{opt}, using: $Q_{in} = JV - Q_{opt}$. During thermal measurements, the devices were suspended several millimeters above an optical table held at ambient temperature. The gap between the table (which acted as an ambient heat sink) and the

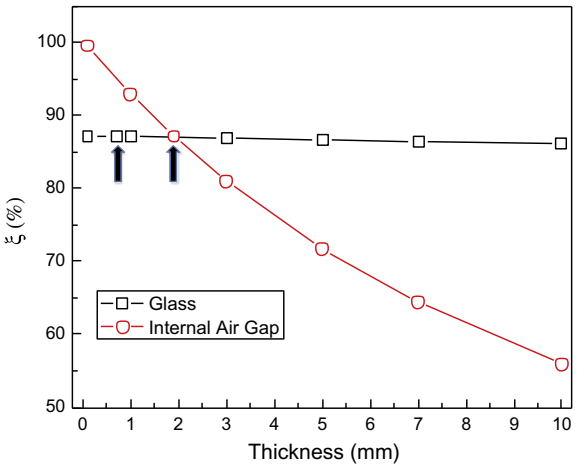

Fig. 3. Calculated fraction (ξ) of steady-state heat dissipated at a thermal input power of 114 W/m^2 via conduction through the bottom device surface vs. thickness of the glass cap and substrate layers (squares) and the internal air gap (circles). Arrows indicate values for the layers in the experimental device in Table 1 and Fig. 2. The operating conditions correspond to a luminance of 3000 cd/m^2. The largest fraction of generated heat is dissipated through conduction, with the thickness of the internal air gap presenting significant thermal impedance to heat transfer. The steady-state temperature increases as the fraction of heat dissipated through highly efficient conduction decreases. The efficiency of convective and radiative cooling also increase with device temperature.

device was too narrow to allow for convection, and hence was treated as an additional thermally conductive layer.

The OLED surface temperature was measured as a function of time at several different current densities after the onset of a current step at $t = 0$ and then compared to model calculations, as shown in Fig. 2. The model is defined by only the thermal parameters of the various layers and the geometry of the setup (see Table 1). The operating currents at the highest intensities result in a surface luminance of ~3000 cd/m^2, with an external quantum efficiency of approximately 19% at all current densities studied.

The accuracy of the model suggests that it can be useful in designing devices with optimized thermal characteristics. In Fig. 3 we plot the fraction of heat dissipation (ξ) via conduction through the bottom device surface vs. the total heat loss, as a function of thickness of the layers (i.e. the glass package cap, squares; or the internal air gap between cap and cathode, circles) between the emission region and the conductive bottom surface. The simulations were performed for a constant input power of 114 W/m^2 that is applied at $t = 0$. Arrows in Fig. 3 correspond to thicknesses of the measured device. The discrepancy between heat dissipation through the two surfaces can be partly explained by the device structure, as shown below, and partly through the different heat transfer mechanisms through the top and bottom surfaces.

Changing the glass cap thickness does not substantially change ξ. It is apparent that heat is primarily dissipated via conduction in the packaged device, and that natural convection to the ambient is a comparatively inefficient heat removal pathway. The efficiency of heat removal through

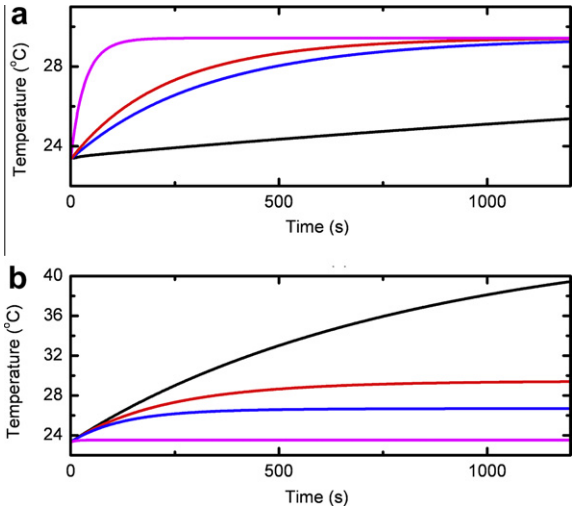

Fig. 4. (a) Effects of thickness of the glass substrate and cap layers. From top to bottom, lines correspond to individual layer thicknesses of 0.1, 0.7 (actual thickness), 1.0, and 10 mm. Variation in glass thickness changes the rate of thermal equilibration, but does not significantly affect the ultimate equilibrium temperature. The 10 mm simulation did not fully reach equilibrium on the time scale shown. (b) Effects of changing the encapsulated air gap thickness. From top to bottom, lines correspond to a thickness of 10, 1.9 (actual thickness), 1.0, and 0.1 mm. For the thinnest layers, there is no significant heating of the device. Devices were modeled for an input thermal power of 114 W/m^2, assumed to be turned on at time $t = 0$.

the top surface of the device is, therefore, limited by convection which is not readily adjusted through changes in device architecture. Forced convection could increase the cooling efficiency, albeit at the risk of increasing lighting fixture cost and complexity.

The bottom device surface also has potential for increased heat extraction via conduction to the ambient. The glass cap and the internal air gap thickness have large effects on heat transfer, as they are by far the thickest layers. Using the same assumptions as in Fig. 3, we modeled the effect of changes in the thickness of these layers on device heating, with the results shown in Fig. 4a. We find that the thicknesses of the glass layers do not have a significant effect on the steady-state temperature. Instead, the thickness of the glass determines the thermal equilibration rate following the onset of device heating. In contrast, the internal air gap (Fig. 4b) presents the most significant bottleneck to heat transfer. For the thinnest air layers considered, (0.1 mm), there is almost no heating predicted for the device at 3000 cd/m^2. This corresponds to a larger percentage of heat being removed through conduction via the bottom surface, as seen in Fig. 3, suggesting that optimal device architectures can operate at room temperature; a highly promising result for the future commercialization of OLEDs for lighting applications.

When the internal air gap limits thermal diffusion, the gap between the bottom surface of the device and the heat-sink must also contribute to device heating. Indeed, we found that the thickness of the air gap has a significant effect on operating temperature, as predicted by the model. Also, the device showed a temperature rise of approximately 1.5 °C when attached directly to a Cu heat-sink. This indicates the existence of an heat-transfer bottleneck due to the internal air gap.

While simulations were performed for a green PHOLED, lighting applications require white PHOLEDs. Nevertheless, we can extend the analysis to white PHOLEDs using data of Levermore et al. [4]. There, an input power of 489 W/m^2 resulted in a brightness of 3000 cd/m^2, as compared to the input electrical power of 132 W/m^2 for the green devices. If we assume identical device structure with an equivalent percentage of input electrical power dissipated as heat, then this device gives a steady-state temperature of 47.8 °C. A temperature rise of approximately 10 °C was reported, suggesting the panel, in that case, was used with a heat sink.

In summary, we have extended the transmission matrix method for modeling heat transfer in OLEDs, providing a full analytical treatment that includes free convection, conduction and radiation. The model accurately predicts the thermal profile of OLEDs while providing an understanding of the factors that determine device operating temperature. In particular, we find that the internal air gap between the package lid and substrate provides the largest impedance to heat transfer, and that elimination of this gap allows operation at near ambient temperature even at high brightness. Further optimization of the thermal performance of OLEDs and other photonic devices can be obtained using the methods presented.

Acknowledgements

We thank the US Department of Energy, Center for Energy Nanoscience at the University of Southern California (award DE-SC0001011, K.B., experiment, analysis), the National Science Foundation SOLAR program (R.K. and S.R.F., analysis), and a Small Business Innovation Research program subcontract funded by the US Department of Energy through Universal Display Corporation (SRF, experimental methods, technology transfer) for financial support.

References

[1] C. Adachi, M.A. Baldo, M.E. Thompson, S.R. Forrest, Journal of Applied Physics 90 (10) (2001) 5048.
[2] B.W. D'Andrade, S.R. Forrest, Advanced Materials 16 (18) (2004) 1585.
[3] Brian W. D'Andrade, James Esler, Chun Lin, Vadim Adamovich, Sean Xia, Michael S. Weaver, Raymond Kwong, Julie J. Brown, Proceedings of SPIE 7051 (1) (2008) 70510Q.
[4] P.A. Levermore, A.B. Dyatkin, Z.M. Elshenawy, H. Pang, J. Silvernail, E. Krall, R. Kwong, M.S. Weaver, R. Ma, J.J. Brown, X. Qi, S.R. Forrest, Journal of Photonics for Energy 2 (2012) 021205.
[5] Xiangfei Qi, Stephen R. Forrest, Journal of Applied Physics 110 (12) (2011) 124516.
[6] Louis A. Pipes, Journal of the Franklin Institute 263 (3) (1957) 195.
[7] Y. Jin, A. Yadav, K. Sun, H. Sun, K.P. Pipe, M. Shtein, Applied Physics Letters 98 (9) (2011) 093305.
[8] Theodore L. Bergman, Adrienne S. Lavine, David P. DeWitt, Frank P. Incropera, Introduction to Heat Transfer, sixth ed., Wiley, 2011.
[9] R.H.S. Winterton, Contemporary Physics 40 (3) (1999) 205.
[10] William M. Haynes (Ed.), CRC Handbook of Chemistry and Physics, 92nd ed., CRC Press, 2011, p. 2656.
[11] M.L. Baesso, J. Shen, R.D. Snook, Chemical Physics Letters 197 (3) (1992) 255.